6th Congress of Alps-Adria Acoustics Assosiation
16.-17. October 2014
Graz, Austria

Austrian Acoustics Association
Österreichische Gesellschaft für Akustik

Alps Adria Acoustics Association

ISBN: 978-3-200-03921-6

CHARACTERIZATION OF THE ACCMF-SYSTEM FOR A SIMULTANEOUS CALIBRATION TECHNIQUE

Jochen Metzger[1], Hendrik Husstedt[2], Manfred Kaltenbacher[1]

[1]Vienna University of Technology
Getreidemarkt 9
1060 Vienna, Austria
jochen.metzger@tuwien.ac.at
manfred.kaltenbacher@tuwien.ac.at

[2]Deutsches Hörgeräte Institut GmbH
Bessemerstraße 3
23562 Lübeck, Germany
h.husstedt@dhi-online.de

Abstract: *The Microflown **U**ltimate **S**ound **P**robe (USP) is an acoustic vector sensor capable of measuring the acoustic intensity in 3D and consists of a pressure microphone and a 3D particle velocity sensor. In order to perform a calibration of all three orthogonally positioned components of the particle velocity sensor simultaneously, we calibrate the USP by means of a reference velocity field above a vibrating piston in an ordinary room without anechoic conditions. During measurements and in this simultaneous calibration procedure it is a matter of importance to know the orientation of the USP. Therefore, a 3D-acceleration sensor and the USP are combined to the **ACC**eleration **M**icro**F**lown (ACCMF)-System. In this paper we present a characterization of the ACCMF, where the 3D-acceleration sensor and the USP are analysed concerning the orientation of the axes and the sensitivity of each component of the sensors. Furthermore, we compare our calibration results with the manufacturer's. Microflown performs the calibration of the USP with the **P**iston **O**n a **S**phere (POS) calibrator and is not able to calibrate the whole frequency range of interest at once and all three components simultaneously. This POS calibration procedure only provides nine calibration parameters, which were obtained from a least square fit of a sensitivity model. For a proper comparison of our obtained calibration results to the POS calibration data, the post processing of the POS calibration procedure is performed by an own implementation of the evaluation process. ACCMF aided calibration results are compared to the results of the POS calibration technique and deviations of the two different calibration procedures are discussed.*

Keywords: calibration, pv-probe, acoustic measurement

1. INTRODUCTION

Since the invention of the Microflown sensor [1, 2], a Micro-Electro-Mechanical-System (MEMS) device, it is possible to measure the acoustic particle velocity in a direct way. With the USP, which can be seen in Fig. 1 a), consisting of three orthogonally positioned components of the particle velocity sensor (x^{MF}, y^{MF}, z^{MF}) and the pressure microphone, a sensor is realized capable for determining 3D particle velocity, sound pressure, impedance [3] , 3D sound intensity [4] and sound energy [5]. In this paper, we analyse the introduced measurement system ACCMF, a combination of a Microflown USP and a 3D acceleration sensor [6, 7]. The ACCMF is analysed concerning the orientation and the sensitivity of each sensor's component. Furthermore, an analysis of the simultaneous calibration procedure is given. Finally, we show and discuss ACCMF aided calibration results in comparison to the calibration results of the manufacturer.

1.1. Working principle of the particle velocity sensor

The working principle of the acoustic particle velocity sensor is depicted in Fig. 1 b). One component of the particle velocity sensor consists of two tiny strips heated by electrical current to an operational temperature between 200 °C and 500 °C. When air flows across the wires from left (orange arrow), wire 1 cools down and the air picks up heat. Wire 2 is cooled down with the heated air. In consequence there is a temperature difference between both wires, which alters their electrical resistance. Due to this operation principle one can

distinguish between positive and negative acoustic particle velocity direction (orange and green arrow). The sensor works in a range of 10 nm/s up to 1 m/s.

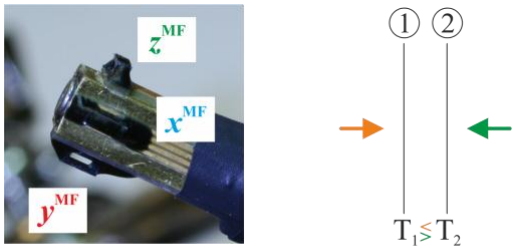

a) b)

Fig. 1. a) USP b) Working principle of the acoustic particle velocity sensor.

1.2. Electric circuit model of the sensitivity

The frequency response of each component of the acoustic particle velocity sensor can be modelled by an electric circuit [8]. This electric circuit, consisting of two high pass filters (*R*1 & *C*1, *R*4 & *C*4) and two low pass filters (*R*2 & *C*2, *R*3 & *C*3) can be seen in Fig. 2 a). The first high pass filter represents the thermal boundary layer on the wires with a corner frequency in the order of $f_1 \approx 100$ Hz. It takes time for heat to travel from one wire to another and this diffusion effect is shown by the first low pass filter with a corner frequency of about $f_2 \approx 1$ kHz. Due to the thermal mass, the temperature of the sensor cannot vary at infinite speed, which is represented by the second low pass filter and a corner frequency in order of $f_3 \approx 10$ kHz. The second high pass corner frequency is about $f_4 \approx 200$ Hz. Thereby, the magnitude frequency response is modeled by

$$|S| = \frac{|S|_{@250\ \mathrm{Hz}}}{\sqrt{1+\frac{f_1^2}{f^2}}\sqrt{1+\frac{f^2}{f_2^2}}\sqrt{1+\frac{f^2}{f_3^2}}\sqrt{1+\frac{f_4^2}{f^2}}} \quad (1)$$

and the phase frequency response by

$$\varphi = \tan^{-1}\left(\frac{c_1}{f}\right) - \tan^{-1}\left(\frac{f}{c_2}\right) - \tan^{-1}\left(\frac{f}{c_3}\right) + \tan^{-1}\left(\frac{c_4}{f}\right). \quad (2)$$

A magnitude and phase response are exemplary shown in Fig. 2 b). $|S|_{@250\ \mathrm{Hz}}$ is the magnitude frequency response at 250 Hz and the constants c_1, c_2, c_3 and c_4 are approximately the same as the corner frequencies f_1, f_2, f_3 and f_4.

1.2. The Piston on a sphere calibration technique

The calibration technique to calibrate the USP by Microflown is the piston on a sphere calibration method [9]. This calibration process is based on known impedance in front of a spherical loudspeaker. According to the manufacturer the usable bandwidth for calibration with the POS is 20 Hz to 20 kHz whereat this frequency range is covered in two steps.

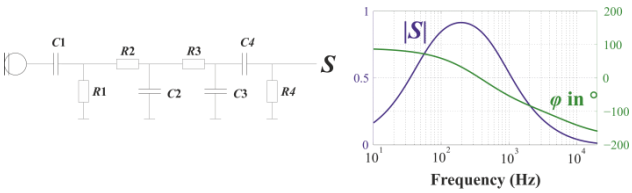

a) b)

Fig. 2. Model of the acoustic particle velocity sensor: a) electric circuit and b) an exemplary magnitude/phase response.

At higher frequencies (200 Hz – 20 kHz) the USP is placed in front of the spherical loudspeaker at nearly the same position as a calibrated reference microphone, see Fig. 3 b). The method is extended to low frequencies (20 Hz – 400 Hz) by measuring the acoustic pressure inside the spherical source and the USP is placed directly in front of the moving membrane, because at low frequencies the acoustic pressure inside the sphere is proportional to the movement of the membrane. This low frequency setup can be seen in Fig. 3 a). Furthermore, the three components of the acoustic particle velocity cannot be calibrated simultaneously. Hence, for the whole calibration procedure six steps are required.

a) b)

Fig. 3. Piston on a sphere: a) low frequency and b) high frequency calibration setup.

The POS speaker is special designed and consists of a hard plastic sphere in which a loudspeaker is placed. This speaker can be modelled with a moving piston with radius b (radius of the moving membrane) on a sphere with radius a. The acoustic impedance, the relation between acoustic pressure and particle velocity in front of a polar cap on a rigid sphere computes with [11]

$$Z_{\mathrm{sphere}}(r) = \lim_{N\to\infty} -j\rho c \frac{\sum_{m=0}^{N}\left(P_{m-1}(\cos\alpha) - P_{m+1}(\cos\alpha)\right)\frac{h_m(kr)}{h'_m(ka)}}{\sum_{m=0}^{N}\left(P_{m-1}(\cos\alpha) - P_{m+1}(\cos\alpha)\right)\frac{h'_m(kr)}{h'_m(ka)}}. \quad (3)$$

In (3) ρ denotes the density of air, c the speed of sound, k the wave number, P_m the legendre function of order m, h_m the spherical hankel function and h'_m its spatial derivative, r the distance from the center of the sphere and $\alpha = \sin^{-1}(b/a)$. Equation (3) calculates very similar to the impedance of a monopole impedance

$$Z_{\text{monopole}}(r) = \rho c \frac{jkr}{1+jkr}. \quad (4)$$

The ratio of impedances (3) and (4) is given in Fig. 4. There is no big difference between both impedances except of the peak at 700 Hz and a major deviation at frequencies around 17 kHz. Additionally, it can be seen that (3) is not very sensitive to the distance variations around $r = 23$ cm. This is very important, because in the high frequency calibration the sensor is placed at a distance of 23 cm in front of the loudspeaker. Because the calibration at high frequencies is done in a range between 200 Hz and 20 kHz in the right part of Fig. 4 only this frequency range is shown.

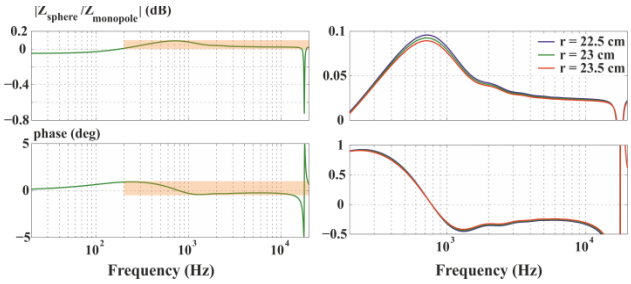

Fig. 4. Ratio of (3) and (4) at a distance of r = 230 mm, radius of the sphere a = 50.5 mm, radius of the piston b = 37.5 mm and N = 50.

The sensitivity in the high frequency calibration procedure of the particle velocity sensor computes with

$$S_{\text{POS}} = \frac{V_{\text{MF}}}{V_{\text{Pref}}} Z_{\text{sphere}} S_{\text{Pref}}, \quad (5)$$

where V_{MF} is the voltage signal of the particle velocity sensor, V_{Pref} is the voltage signal of the reference microphone and S_{Pref} is the sensitivity of the reference microphone.

At frequencies below 400 Hz the background noise has higher pressure levels than the noise generated by the speaker. In the low frequency calibration setup the acoustic pressure p_{ref} inside the sphere is measured. The velocity of the membrane can be calculated with [12]

$$u_{\text{n}} = -\frac{j\omega V_0}{\gamma A_0 p_0} p_{\text{ref}}. \quad (6)$$

In (6) ω denotes the angular frequency, V_0 the interior volume, A_0 the surface of the membrane, p_0 the ambient pressure and γ the ratio of specific heat (1.4 for normal air). The particle velocity in front of the moving membrane at a distance r is given by [11]

$$u(r) = \lim_{N\to\infty} -\frac{u_{\text{n}}}{2} \sum_{m=0}^{N} \left(P_{m-1}(\cos\alpha) - P_{m+1}(\cos\alpha)\right) \frac{h_m'(kr)}{h_m'(ka)}. \quad (7)$$

Using (7), the particle velocity at the USP can be calculated and thus the calibration at lower frequencies can be performed. In a final step the calibration results of both calibration procedure will be combined with an overlap area in the frequency range between 200 Hz and 400 Hz.

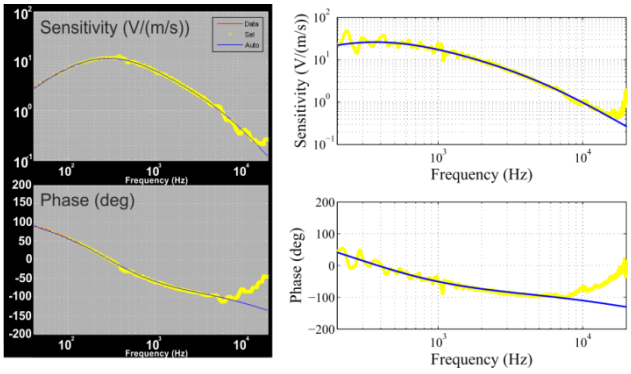

Fig. 5. Calibration results of a POS calibration: on the left the result of the manufacturer software and on the right the evaluation by our own.

An exemplary calibration result of the POS calibration is shown in Fig. 5. The calculated sensitivities and the phase response are displayed as yellow lines. The fit with (1) and (2) is displayed with the blue line. The fitting parameter c_1, c_2, c_3 ,c_4 ,f_1, f_2, f_3 ,f_4 and $|S|_{@250\text{ Hz}}$ for each component of the particle velocity sensor of the USP can be found in the calibration report provided by the manufacturer. With this known sensitivities the measured particle velocity can be corrected, but it is obvious, that there is a difference between the real sensitivity (yellow line) and the model of sensitivity (blue line). This difference can cause measurement errors, especially in the frequency range where the difference between the model and the calculated sensitivity is singificant. A major difference up to 120° in phase and 10 dB in magnitude can be seen between 400 Hz and 500 Hz and at frequencies more than 5 kHz.

2. THE SIMULTANEOUS CALIBRATION TECHNIQUE

The simultaneous calibration technique for the acoustic particle velocity sensor by means of a reference velocity field generated by a vibrating piston was introduced in [6]. As part of this calibration technique, the three components of the acoustic particle velocity sensor can be calibrated without any anechoic conditions over the whole audible frequency range at once. Thereby, the USP is exposed to a sound field generated by a vibrating piston mounted on an electrodynamic vibration exciter. The surface velocity of the piston $\vec{v_r}$ is assumed to be homogeneous, perpendicular to the moving surface and oriented in the same direction as the local gravity field $\vec{g}$. This orientation of the homogeneous assumed reference fields has been verified by mounting the acceleration sensor on the surface of the vibrating piston. The deviation of orientation between $\vec{v_r}$ and $\vec{g}$ is the deviation of the static and dynamic

acceleration vector. This deviation is smaller than 1° and negligible. The velocity on the surface of the vibrating piston is determined by using a laser vibrometer and is controlled to be constant over frequency with relative deviations under one percent of the preset velocity.
A particle velocity sensor is sensitive to the reference velocity field $\overrightarrow{v_r}$ and a acceleration sensor responses to the local gravity field $\vec{g}$. With the assumption that

- both reference fields are antiparallel to each other and perfectly homogeneous,
- the three components of both sensors are perfectly orthogonal and
- the origin of both sensor's coordinate systems are different but the axes are identically orientated,

the effective acoustic particle velocity v_i at each component (i = 1,2,3) can be determined with

$$\frac{a_i}{|\vec{g}|} = -\frac{v_i}{|\vec{v}_r|}, \tag{8}$$

where a_i is the effective acceleration of the i-th component of the acceleration sensor, $\vec{g}$ the local gravity vector and $\overrightarrow{v_r}$ the vector of the reference velocity field.

3. CHARACTERIZATION OF THE ACCMF

The ACCMF, a combination of a 3D acceleration sensor and a particle velocity probe, which can be seen in Fig. 6, was introduced in [7]. By means of this ACCMF it is possible to perform a calibration of the particle velocity sensor as described in section 2. The 3D acceleration sensor used in the measurements is a ADXL330 and the particle velocity probe is a Microflown USP.

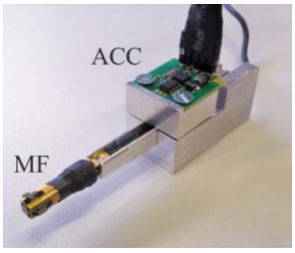

Fig. 6. The ACCMF Measurement system.

3.1. Sensitivity of the acceleration sensor

For determining the sensitivities of the three components (x^{AC}, y^{AC}, z^{AC}) of the acceleration sensor the system of linear equations

$$\begin{bmatrix} M_{x1} & M_{y1} & M_{z1} \\ \vdots & \vdots & \vdots \\ M_{xn} & M_{yn} & M_{zn} \end{bmatrix} = \begin{bmatrix} a_{11} & a_{21} & a_{31} & 1 \\ \vdots & \vdots & \vdots & \vdots \\ a_{1n} & a_{2n} & a_{3n} & 1 \end{bmatrix} \cdot \begin{bmatrix} A_{11} & 0 & 0 \\ 0 & A_{22} & 0 \\ 0 & 0 & A_{33} \\ A_{10} & A_{20} & A_{30} \end{bmatrix} \tag{9}$$

have to be solved. Here [M] is a nx3 matrix of voltage of the acceleration sensor, [a] the nx4 matrix of accelerations and [A] the system matrix with the sensitivities of the three components (A_{11}, A_{22}, A_{33}) and the offsets A_{10}, A_{20} and A_{30}, where n is the number of measurements. With $n \geq 4$, one can solve for the system matrix by using the least square method

$$[A] = (a^{\mathrm{T}}a)^{-1}a^{\mathrm{T}}M = \begin{bmatrix} 0.325 & 0 & 0 \\ 0 & 0.335 & 0 \\ 0 & 0 & 0.320 \\ 1.625 & 1.643 & 1.613 \end{bmatrix} \frac{\mathrm{V}}{\mathrm{g}} \tag{10}$$

and hence determine the sensitivities of the components of the acceleration sensor. The entries of the system matrix were obtained by $n = 6$ measurements. With this characterization of the sensitivities of the acceleration sensor's axes, we get the sensitivity of the acceleration sensor in each direction.

3.2. Numerical Simulation of the reference velocity field

Before an investigation of the orientation of the single components of the both sensors is done, the reference field will be analysed. Both reference fields were assumed to be perfectly homogeneous. However, the velocity field in front of a moving piston is not homogenous. The beam angle strongly depends on the frequency of excitation. The reference velocity field above the moving piston was calculated by a 2D FEM-simulation. The axially symmetric simulation setup and its dimensions are shown in Fig. 7. This simulation setup consists of an excitation line, which represents the excitation via the moving piston and a propagation region, which models the air in front of the piston. The propagation region is surrounded by a perfectly matched layer (PML) [10] for modelling free radiation. The simulation was done with different radius of the moving piston from 15 mm to 40 mm over the whole audible frequency range between 20 Hz and 20 kHz.

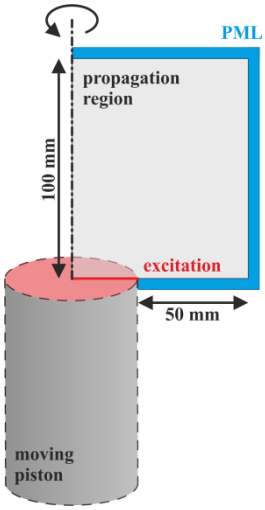

Fig. 7. Axially symetric simulation setup.

The result of the FE simulation can be seen in Fig. 8, where the amplitude of the velocity relative to the amplitude of the excitation is shown. It can be seen, that the sound field is getting more and more inhomogeneous with higher frequenicies. Especially at frequencies above 10 kHz a homogeneous sound field cannot be assumed. Therefore, we use the computed particle velocity field within our calibration procedure.

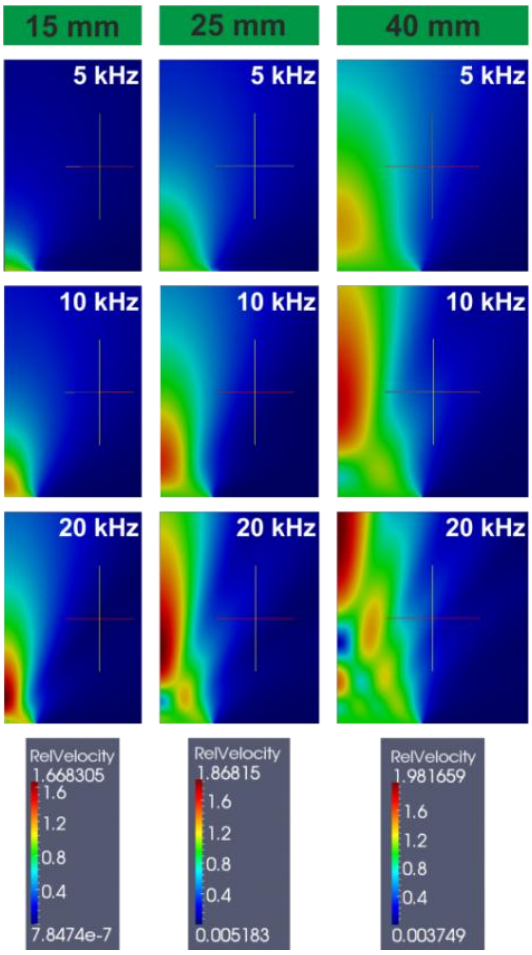

Fig. 8. Simulation results of the relative amplitude of acoustic particle velocity infront of the moving piston with radius 15 mm, 25 mm and 40 mm at 5 kHz, 10 kHz and 20 kHz.

3.3. Orientation of the ACCMF sensor's components

To identify the orientation of the sensor's components, we rotate the ACCMF around each pair of parallel axes in the reference field. The measurement setup and the expected signals from both other axes for a rotation around the *z*-axis of both sensors are displayed in Fig. 9. The signals of the sensors' components should be shifted. If the axes of one sensor are perfectly orthogonal, the phase shift of the two signals (e.g. between x^{MF} and y^{MF}) of the sensor's components should be exactly 90°. Between the parallel assumed sensor components of each sensor (e.g. between x^{MF} and x^{AC}) there should be a phase shift of 180°, because the reference fields are antiparallel to each other.

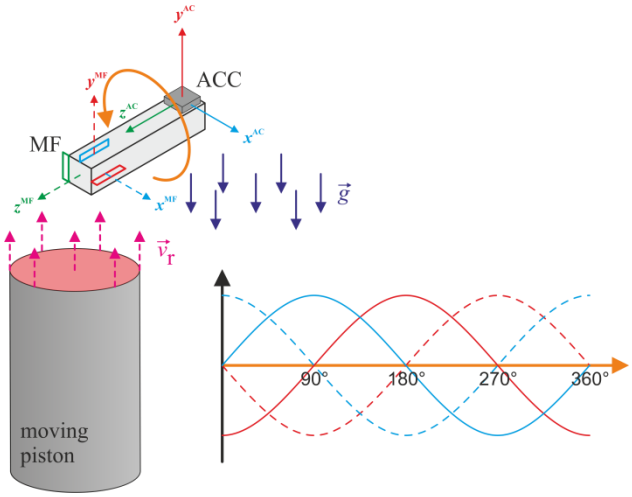

Fig. 9. Measurement setup to identify the orientation of the ACCMF sensor's components (not to scale!).

As can be seen in Fig. 9, it is very easy to turn the ACCMF-system around the *z*-axes, but there is a problem with the other axes. The angles of rotation around the *x*- and the *y*-axes are limited to 180°. Moreover the signals shown in Fig. 9 either require a rotation of one component of the particle velocity around a point or a rotation in a homogeneous velocity field. The analysis of the orientation was performed at 500 Hz with a piston radius of 40 mm at two different distances of 2.25 cm and 4.5 mm in front of the moving piston. As shown in the numerical simulation of the reference velocity field we cannot assume a homogeneous field in front of the moving piston. Additionally the components of the particle velocity sensor does not turn around a point, but they describe a circle with radius 2.5 mm. In Fig. 10 the velocity distribution at 500 Hz and two circles at the different distances are shown. Furthermore, the velocity relative to its maximum at 180° at the two different distances to the surface of the moving piston are displayed.

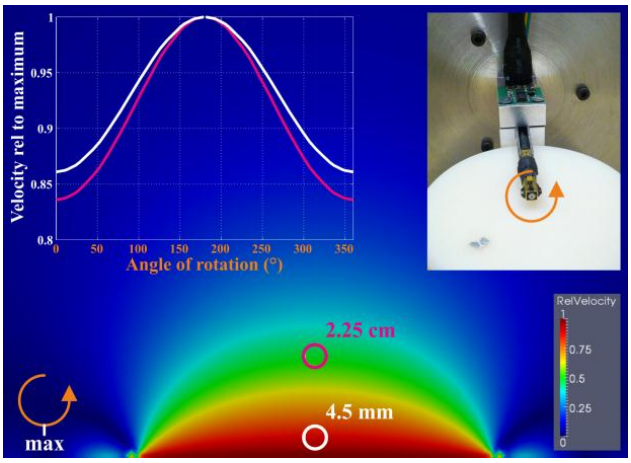

Fig. 10. Velocity distributuion in front of the moving piston with radius 40 mm at 500 Hz. The plot shows the velocity relative to the maximum at 180°.

The deviation from the perfect orthononality of the acceleration sensor is shown in Tab. 1. It is obvious that the acceleration sensor is not perfectly orthogonal but the deviation from 90° are very small.

Axes	$x^{AC} - y^{AC}$	$x^{AC} - z^{AC}$	$y^{AC} - z^{AC}$
Deviation	0.0186°	0.0562°	0.2339°

Table 1. Determined deviation from perfect orthononality of the used acceleration sensor.

In Tab. 2 the deviation from 90° phase shift between the axes of the particle velocity sensor is listed. The determination revealed much more deviation of the particle velocity sensor from perfect orthogonality than the deviation of t–he acceleration sensor. However, the measurements of the angle between *x*- and *y*-axis must be more robust, because the total angle of rotation is not limited to 180°.

Axes	$x^{MF} - y^{MF}$	$x^{MF} - z^{MF}$	$y^{MF} - z^{MF}$
Deviation	1.37°	9.38°	4.62°

Table 2. Determined deviation from perfect orthononality of the particle velocity sensor in the USP.

For a better understanding of rotation limit to 180°, the start- and end-szenario of a rotation around the *x*- and *y*-axes are shown in Fig. 11.

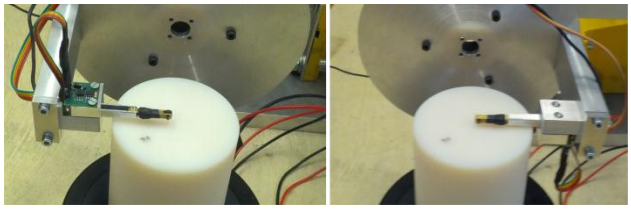

Fig. 11. Limitation of the angle of rotation in the rotation around the *x*- and *y*-axes.

In Tab. 3 the orientation deviation of both sensors are listed. It can clearly be seen, that the determined deviation from a perfect parallel orientation of the *x*-axes and the *y*-axes of both sensors are much smaller than the devation of the *z*-axes, because of the problem not being able to turn the ACCMF with more than 180°.

Axes	$x^{MF} - x^{AC}$	$y^{MF} - y^{AC}$	$z^{MF} - z^{AC}$
Deviation	0.62°	2.36°	5.57°

Table 3. Determined deviation from perfect perfect orientation of both sensors

Nevertheless, the most important point from the analysis of orientation of both sensors is that the sensors are nearly orientated in the same direction with a deviation at maximum of 5.57°. This orientation deviation can result in errors calculating the velocity at each component of the particle velocity sensor with (8).

4. CALIBRATION RESULTS

In Fig. 12 the sensitivity of the x^{MF} component of the USP can be seen. The sensitivity was determined by the simultaneous calibration technique described in section 2. The calibration was done with different radius of the moving piston (15 mm, 25 mm and 40 mm). The sensitivity's magnitude and phase response is compared to the sensitivity, determined by the POS calibration routine. It can be seen, that the trend of the two calibration results is similar although there is a main deviation in magnitude and phase response at very high frequencies over 10 kHz. It can clearly be seen, that the phase response determined with the simultaneous calibration technique is less than the phase response determined with the POS calibration technique. Furthermore the sensitivities determined with the various piston geometries are different. The magnitude in R15 seems to be shiftet over the whole frequency in comparison to the magnitude of R25 and R40. Additionally there are peaks in magnitude and phase response which make no sense in a physical point of view. These peaks could be avoided by using a filter, e.g. a moving average. It is obvious that the phase of the own implemented post processing of the POS calibration process coincides more to the obtained results by the simultaneous calibration technique than the sensitivity model at frequencies up to 200 Hz.

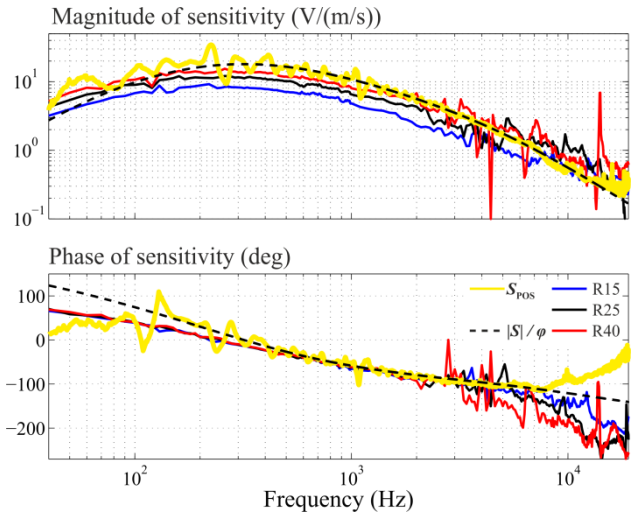

Fig. 12: Magnitude and phase of the sensitivity determined with different piston in comparison to the nominal correction curve and the own calibration evaluation with (5).

5. CONCLUSION

In this paper a full characterization of the ACCMF system is presented in order to perform a simultaneous calibration

of all three components of the acoustic particle velocity sensor of the USP. The orientation analysis of two pair of axes gives reliable results. The analysis of the third pair of axes provides a potential for improvement, because the ACCMF system cannot be rotated more than 180° around the *x*- and the *y*-axes. Further investigation will be done to be able to analyse all axes orientation. Moreover, the calibration results obtained by the simultaneous calibration technique are in a good agreement in comparison to the sensitivity determined by our own post processing of the POS calibration.

6. ACKNOWLEDGEMENT

We gratefully thank Microflown for providing the POS calibration data especially Lola Garcia for her great support.

REFERENCES

[1] H.E. de Bree et al.: ***Novel device measuring acoustical flows***, *Proceedings of International Conference on Solid-State Sensors and Actuators & Eurosensors IX*, 54(1-3), 1995, 536-539.

[2] H.E. de Bree et al.: ***The µ-flown: a novel device for measuring acoustic flows***, *Sensors and Actuators*, 54(1-3), 1996, 552-557.

[3] R. Lanoye et al.: ***Measuring the free field acoustic impedance and absorption coefficient of sound absorbing materials with a combined particle velocity-pressure sensor,*** *Journal of the Acoustical Society of America*, 119(5), 2006, 2826-2831.

[4] E. H. G. Tijs et al.: ***Rapid high resolution 3D intensity measurement with a stereo camera system,*** *Proceedings of DAGA 2014: 40. Jahrestagung für Akustik*, Oldenburg, 2014, 628-629.

[5] D. B. Nutter et al.: ***Measurement of sound power and absorption in reverbation chambers using energy density,*** *Journal of the Acoustical Society of America*, 121(5), 2007, 2700-2710.

[6] J. Metzger, M. Kaltenbacher: **Simultaneous calibration of all three acoustic particle velocity components of a pressure-velocity probe**, *Proceedings of 42nd International Congress and Exposition on Noise Control Engineering 2013, INTER-NOISE 2013: Noise Control for Quality of Life*, Innsbruck, 2013, 3838-3844.

[7] J. Metzger, M. Kaltenbacher: ***Simultane Kalibrierung der drei Komponenten des Schnellesensors einer pv-Sonde mit Hilfe eines schwingenden Kolbens***, *Proceedings of DAGA 2014: 40. Jahrestagung für Akustik*, Oldenburg, 2014, 638-639.

[8] V.B. Svetovoy, I.A. Winter et al.: ***Model of the Microflown microphone,*** *Sensors and Actuators*, 86(3), 2000, 171-181.

[9] T. Basten, H.E. de Bree: ***Full bandwidth calibration procedure for acoustic probe containing apressure and particle velocity sensor***, *Journal of the Acoustical Society of America*, 127(1), 2010, 264-270.

[10] B. Kaltenbacher, M. Kaltenbacher, I. Sim.: ***A modified and stable version of a perfectly matched layer technique for the 3-d second order wave equation in time domain with an application to aeroacoustics,*** *Journal of Computational Physics*, 235, 2013, 16 p..

[11] E.G. Williams: ***Fourier Acoustics: Sound Radiaton and Nearfield Acoustic Holography***, *Academic Press*, London, 1999.

[12] F. Jacobsen, V. Jaud: ***A note on the calibration of pressure-velocity sound intensity probes***, *Journal of the Acoustical Society of America*, 120(2), 2006, 830-83.